

Journal of **Materials Chemistry C**

Non-Kelulé Copolymer Films for Optoelectronics

Journal:	Journal of Materials Chemistry C
Manuscript ID	TC-ART-08-2024-003420.R1
Article Type:	Paper
Date Submitted by the Author:	09-Nov-2024
Complete List of Authors:	Wu, Niannian; RIKEN, CEMS Mitoma, Nobuhiko; RIKEN, CEMS Mori, Shunsuke; RIKEN, CEMS Chiew, Yi Ling; RIKEN, CEMS Yu, Xiuzhen; RIKEN, CEMS Oshima, Yugo; Rikagaku Kenkyujo, Wang, Shuxu; RIKEN, CEMS Liu, Jinxu; RIKEN, CEMS Aida, Takuzo; The University of Tokyo, Department of Chemistry and Biotechnology

SCHOLARONE™ Manuscripts

PAPER

Non-Kelulé Copolymer Films for Optoelectronics

Niannian Wu,^{ab} Nobuhiko Mitoma,^{*ab} Shunsuke Mori,^a Yi Ling Chiew,^a Xiuzhen Yu,^a Yugo Oshima,^c Shuxu Wang,^{ab} Jinxu Liu^{ab} and Takuzo Aida^{*ab}

Received 00th January 20xx, Accepted 00th January 20xx

DOI: 10.1039/x0xx00000x

We investigate the synthesis and properties of a photoactive copolymer film, gCN-co-gC, which integrates graphitic carbon (gC) domains into a graphitic carbon nitride (gCN) network. The film, produced via vapor-deposition copolymerization of melamine and glucose, addresses two significant challenges of gCN: limited optical absorption range and poor processability. As the amount of gC increases, the gCN-co-gC film shows enhanced optical absorption, extending into the visible light spectrum (>400 nm), and improved electrical conductivity, making it suitable for optoelectronic applications. The study also revealed that gCN-co-gC posesses stable radicals even in the dark at room temperature. This suggests that the open-shell non-Kelulé structure disrupt electron-hole recombination, realizes metal-free paramagnetic copolymers.

Introduction

Graphitic carbon nitride (gCN) is a crosslinked polymer of heptazine (also known as tri-s-triazine), which comprises sp² carbon and sp² nitrogen atoms. Its valence and conduction bands originate from the energy levels of 2pz orbitals of nitrogen and carbon, respectively^{1,2}. Upon light irradiation, electrons in gCN are excited and transferred from its valence band to the conduction band. In 2009, Wang, Domen, and Antonietti et al. discovered for the first time that gCN functions as a metal-free photocatalyst for water splitting¹. When gCN is placed in an aqueous medium, its holes oxidize water (2H₂O → O_2 + 4H⁺ + 4e⁻) and its electrons reduce protons (2H⁺ + 2e⁻ \rightarrow H₂). The extension of gCN into optoelectronic applications beyond photocatalysis has long been anticipated due to their non-metallic composition, modulable energy band structure, and excellent chemical stability. However, the applications of gCN face two challenges: (1) a narrow optical absorption range of ~365 nm1, makes it difficult to utilize inexhaustible solar energy³, and (2) powdery form⁴ that neither dissolves in any organic solvent nor melts upon heating, makes it difficult to postprocess into desired shapes such as thin films.

In this study, we report a photoactive copolymer film of gCN and graphitic carbon (gC), named gCN-co-gC to address the two above-described challenges simultaneously. This film was directly fabricated on a target substrate via the simultaneous vapor-deposition copolymerization (VDP) of melamine and

glucose, and characterized by its high structural integrity. In 2016, we reported the first self-supporting gCN film via VDP of guanidinium carbonate⁵. Although this gCN film had high structural integrity and was essentially different from the sintered films of gCN powder, it was not a fracture-less material. In 2020, this problem was nearly solved by using a tube furnace with low- and high-temperature zones that enabled VDP of melamine under a nitrogen flow⁶. The poor continuity of sintered films composed of gCN powder^{7,8}, which has hampered the development of gCN as a photoelectronic material, has been addressed by the VDP method. Now, how can we expand the optical absorption range of gCN? We were inspired by the pioneering work of Che et al. on the formation of gC-hybridized gCN powder9. gC-hybridization provides gCN with new energy states in its energy band gap and allows for enhancing the optical absorption. They utilized this powdery material for photochemical water splitting and reported that its efficiency was 10 times higher than that of the pristine gCN powder, although the light with a wavelength shorter than 400 nm was still a main contributor to the photochemical water splitting. In the present paper, we employed a mixture of melamine and glucose for VDP to obtain a photoresponsive film for visible light (>400 nm).

Results and discussion

We synthesized gCN-co-gC via a dual-zone VDP process. To fabricate gCN-co-gC with a gC carbon content of 37 atomic%, a powdery mixture of melamine (0.95 g, 7.53 mmol) and glucose (0.05 g, 0.27 mmol) was placed in a 13.5-mL glass vial in a quartz tube (1 inch in diameter) surrounded by a tube furnace. The tube furnace comprised two zones at different temperatures, where the glass vial containing the precursor mixture was placed in the lower-temperature zone and the temperature of the other zone was fixed at 550 °C. Upon flowing argon gas at

^{a.} RIKEN Center for Emergent Matter Science, 2-1 Hirosawa, Wako, Saitama 351-0198, Japan.

b. Department of Chemistry and Biotechnology, The University of Tokyo, 7-3-1 Hongo, Bunkyo-ku, Tokyo 113-8656, Japan.

^c RIKEN Cluster for Pioneering Research, 2-1 Hirosawa, Wako, Saitama 351-0198, Japan.

 $[\]hbox{* Corresponding authors: nobuhiko.mitoma@riken.jp, aida@macro.t.u-tokyo.ac.jp}\\$

[†] Supplementary Information available: [Materials and Methods]. See DOI: 10.1039/x0xx00000x

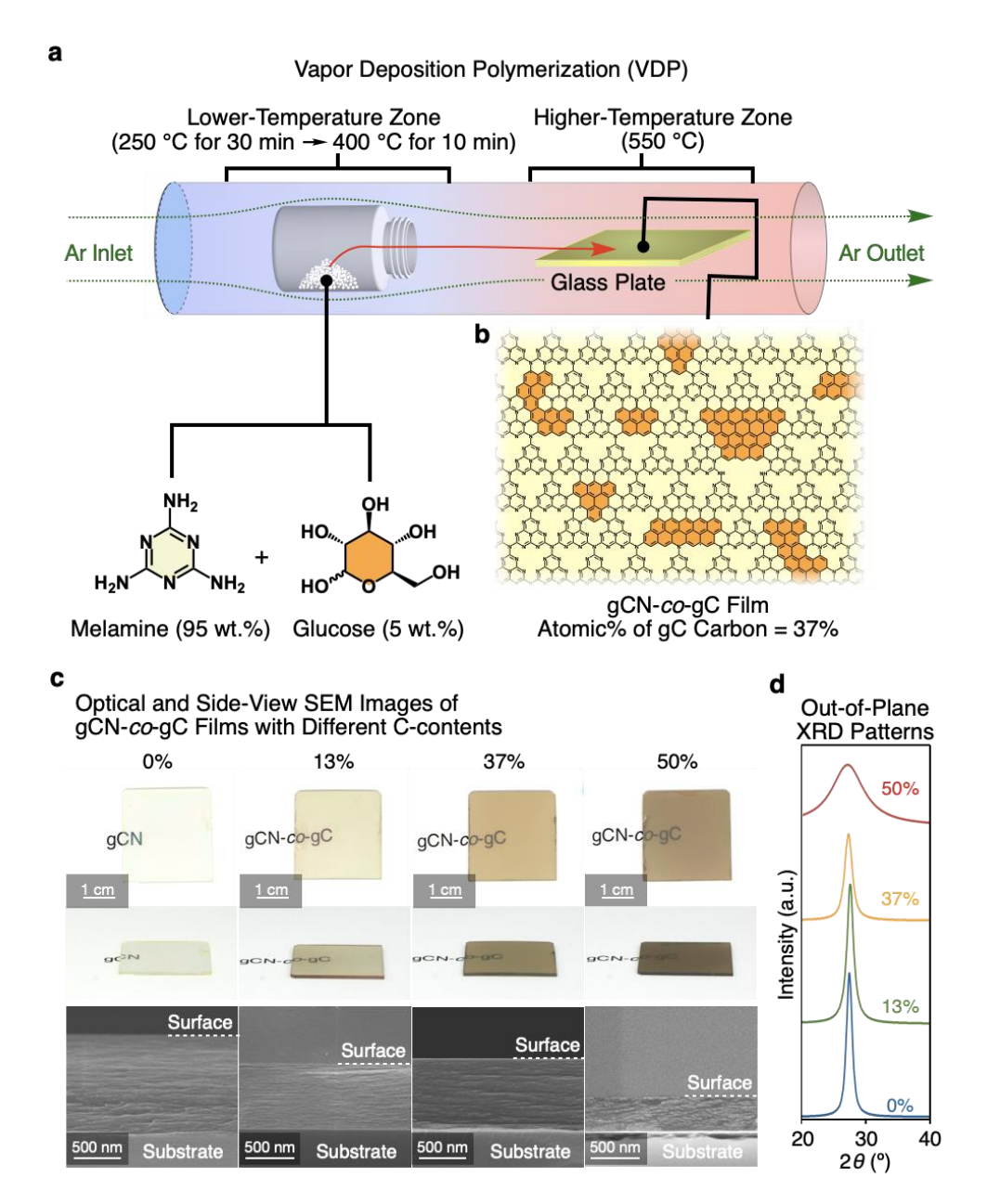


Fig. 1 | **gCN-***co*-**gC** films prepared by VDP. (a) Schematic representation of the two-zone VDP experimental setup to synthesize gCN-*co*-gC films comprising the gCN network and gC domains onto a target substrate, where the melamine–glucose mixture was used as the precursor compound. (b) Schematic representation of the structure of gCN-*co*-gC 37%. (c) Optical and sideview SEM images of gCN-*co*-gC with different C-contents. (d) Out-of-plane XRD patterns of gCN and gCN-*co*-gC 13%, 37%, and 50%.

a rate of 25 mL min⁻¹, the precursor mixture, initially heated at 250 °C for 30 min, was heated up to 400 °C and the product was deposited on the target substrate in the higher-temperature zone. After 10 min, the tube furnace was rapidly cooled to room temperature (~25 °C) to terminate the reaction (Fig. 1a, Supplementary Fig. 1). The resulting films of gCN-co-gC had a uniform appearance, but their color darkened as the glucose content in the precursor mixture increased (Fig. 1c) from 0 to 2, 5, and 10 wt.%, where the gC carbon content (atomic%) of the resulting gCN-co-gC films increased to 13, 37, and 50%, respectively, as confirmed by X-ray photoelectron spectroscopy

(XPS; Supplementary Fig. 2). Other than gCN-co-gC 50%, the films exhibited a layered stacking structure analogous to that of pristine gCN film, as confirmed by scanning electron microscopy (SEM; Fig. 1c) and X-ray diffraction (XRD; Fig. 1d). In particular, the XRD patterns of gCN-co-gC 13% and 37% showed sharp diffractions at $2\vartheta \simeq 27.6^\circ$ and 27.3° , respectively, assignable to the (002) plane of gCN¹⁰; however, due to structural disordering, the XRD pattern of gCN-co-gC 50% exhibited a broad diffraction centered at $2\vartheta \simeq 27.2^\circ$.

Journal of Materials Chemistry C

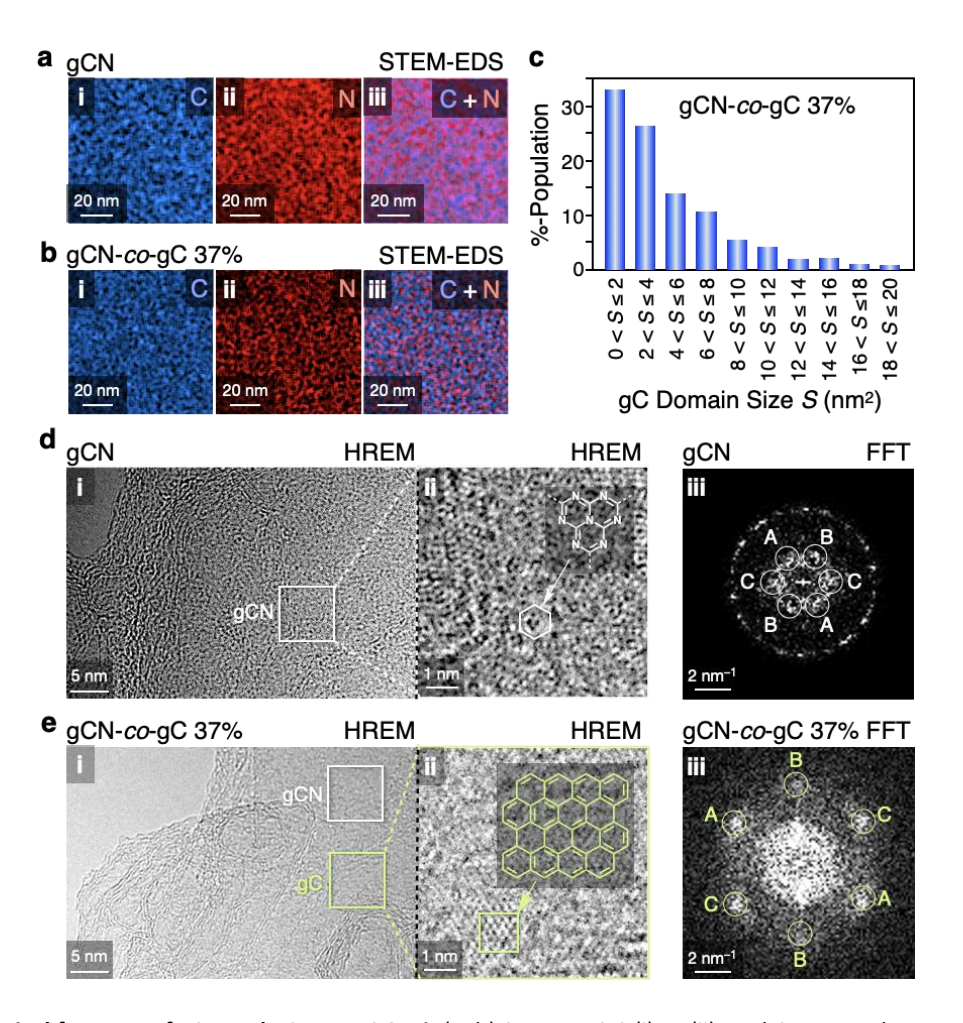


Fig. 2| Morphological features of gCN and gCN-co**-gC 37%.** (a, b) STEM-EDS C (i), N (ii), and C + N overlay mapping images (iii) of gCN and gCN-co-gC 37%. (c) Histogram of the size distribution of the gC domains in gCN-co-gC 37%. (d, e) HREM images (i, ii) and FFT patterns (iii) of gCN (d_A = 0.58 nm, d_B = 0.59 nm, d_C = 0.55 nm) and gCN-co-gC 37% (d_A = 0.20 nm, d_B = 0.20 nm, d_C = 0.20 nm). d_A , d_B , and d_C are the lattice spacing.

For investigating the homogeneity in gCN-co-gC, we employed scanning transmission electron microscopy (STEM) combined with energy dispersive X-ray spectroscopy (EDS). By EDS mapping of gCN (Fig. 2a), we confirmed that the signals from carbon (C) and nitrogen (N) were uniformly distributed as expected^{9,11}. In contrast, the EDS mapping of gCN-co-gC 37% showed a uniform distribution of the C signal originating from both gCN and gC (Fig. 2b [i]) but the N signal, which originated only from gCN, was deficient in some local areas (Fig. 2b [ii]), indicating that the gC domains were dispersed in the gCN network (Figure 1b). For nanostructure visualization of gCN-cogC, we employed high-resolution transmission electron microscopy (HREM; Figs. 2d [i, ii], 2e [i, ii]). A gCN film in HREM imaging exhibits partially displayed heptazine units, as highlighted by the open hexagon in Fig. 2d [ii]. Consistent with the STEM-EDS results, the HREM image of gCN-co-gC 37% (Fig. 2e [i]) exhibited two distinct areas composed of gCN (open white square) and gC (open green square). The fast Fourier transform (FFT) analysis of the HREM images clearly showed a hexagonal pattern both for gCN (Fig. 2d [iii]) and gCN-co-gC 37%

(Fig. 2e [iii]), indicating that not only the gCN network but also the gC domains dispersed in the gCN network are oriented parallel to the in-plane direction of the film. Particularly, the gCN network (white circles, Fig. 2d [iii]) clearly showed a sixfold reflection, indicating that heptazine adopts a long-period structural order with a plane distance of ~0.6 nm¹². Meanwhile, the hexagonal pattern of gC domains dispersed in the gCN network (green circles, Fig. 2e [iii]) showed a short-period structural order with a calculated lattice spacing of ~0.2 nm, matching the lattice constant of the (100) plane of graphite¹³. Then, we analyzed the gC domain size distribution of gCN-co-gC 37% (Fig. 2c), and obtained a bar chart, whose size distribution followed a Poisson distribution. In contrast, the size distribution of gC domains in gCN-co-gC 50% deviated from Poissonian (Supplementary Fig. 5).

To investigate whether the gC domains are covalently connected to the gCN network, we analyzed the film samples of gCN, gCN-co-gC 13%, 37%, and 50% with XPS. As shown in Fig. 3a, the C 1s XPS spectrum of gCN can be deconvoluted into three peaks, at 288.7, 286.5, and 284.8 eV, which were

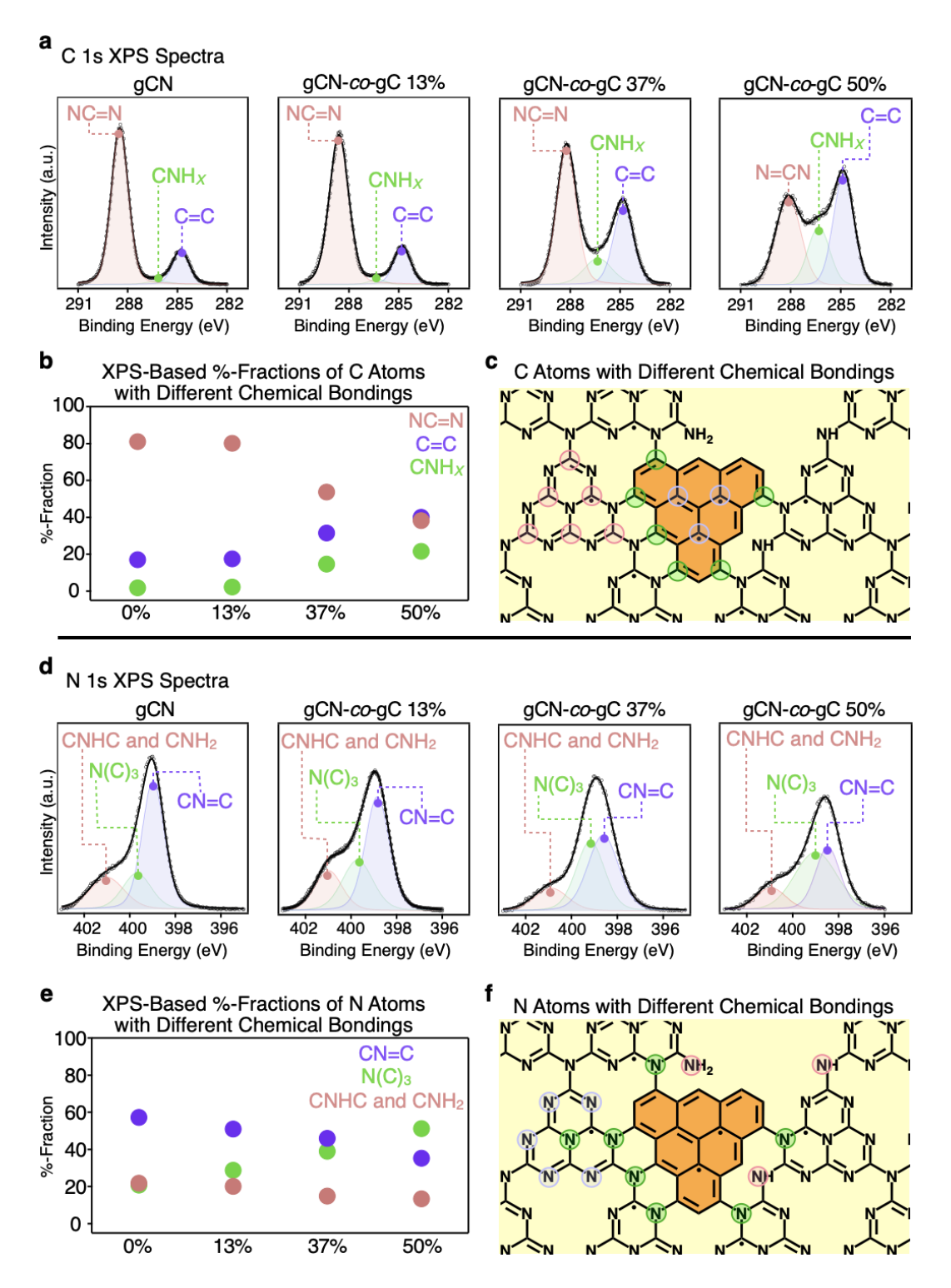


Fig. 3| Chemical structures. C 1s (a) and N 1s (d) XPS spectra of gCN and gCN-co-gC 13%, 37%, and 50%. The XPS-based %-fractions of C 1s (b) and N 1s (e) with different chemical bondings. Scheme structures of gCN-co-gC and the C (c) and N (f) atoms with different chemical bondings.

assignable to sp² hybridized NC=N in heptazine, carbon bonded to amino end groups (CNH $_x$), and aromatic C=C bonds, respectively^{12,14}. After the deconvolution, the C 1s XPS spectrum of gCN-co-gC 37% showed these three peaks, one of which, denoted as "CNH $_x$ ", indicated the existence of covalent

bonds between the gCN network and gC domains (Fig. 3c, green). As the gC content of gCN-co-gC increased from 13% to 37%, the %-fraction of the C atoms in CNH $_x$ increased from 2.3% to 14.7% (Fig. 3b, green). Accordingly, the %-fraction of the C atoms in C=C increased (Fig. 3b, violet) whereas that of the C

atoms in NC=N decreased (Fig. 3b, pink). In the meantime, the N 1s XPS spectrum of gCN after deconvolution showed three peaks, at 401.0, 399.7, and 399.0 eV, corresponding to nitrogen species in CNHC/CNH₂, tertiary N(C)₃, and sp² hybridized CN=C, respectively^{12,14}. When gC domains were incorporated into the gCN network, the %-fraction of N(C)₃ increased due to covalent bond formation (Figs. 3d, 3e, 3f; green) whereas those of CNHC/CNH₂ (Figs. 3d, 3f; pink) and CN=C (Figs. 3d, 3f; violet) decreased. As expected, as the gC content in gCN-co-gC increased from 13% to 37%, the %-fraction of the N atoms in N(C)₃ increased from 28.8% to 39.1% (Fig. 3e, green).

The electronic structure of gCN-co-gC is modulable by the amount and dispersion status of gC domains in the gCN

network. The gCN films showed a characteristic absorption band centered at 365 nm, whose absorption edge was observed at ~450 nm. Consistent with our previous report⁶, the energy bandgap of gCN was 2.76 eV. Meanwhile, the absorption onset of gCN-co-gC was more red-shifted as more gC domains were incorporated into the gCN network (Fig. 4a). The C $2p_z$ orbitals introduce new energy states near the conduction band edge of the parent material gCN, resulting in narrowing the energy band gap⁹. Likewise, the photoluminescence of gCN-co-gC was red-shifted and attenuated as more gC domains were incorporated into the gCN network (Fig. 4b). These findings implied that the π -conjugated electrons in gCN-co-gC were more delocalized than those in gCN¹⁵. Consequently, gCN-co-gC showed an

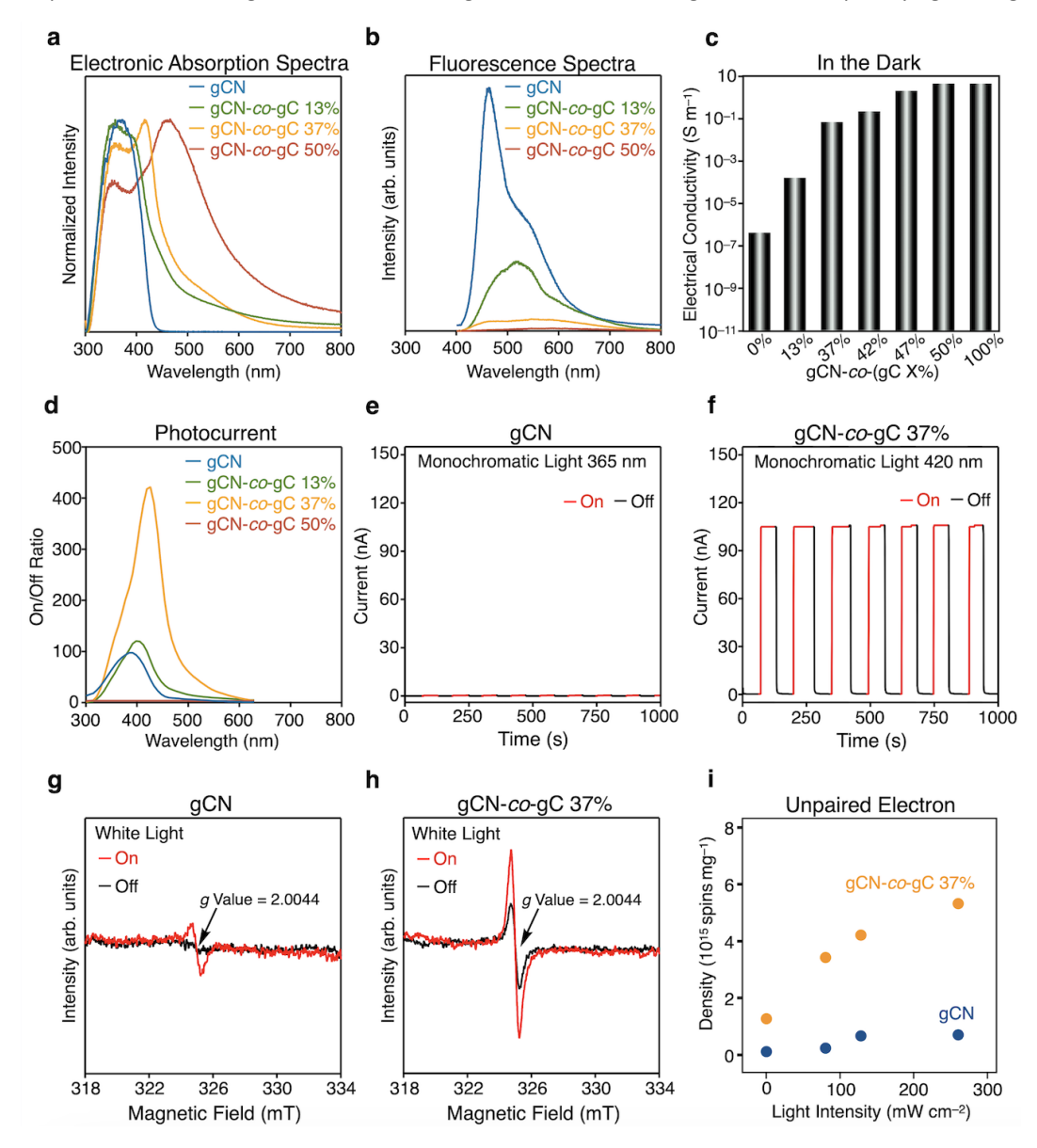


Fig. 4| Electrical and optical properties. Electronic absorption spectra (a) and fluorescence spectra (b) of gCN and gCN-*co*-gC 13%, 37%, and 50%. (c) Electrical conductivity of gCN-*co*-gC with an increasing content of gC domains. (d) Wavelength dependency of the photocurrents of gCN and gCN-*co*-gC 13%, 37%, and 50%. Cycle stability of the photocurrents of (e) gCN (365 nm, 75 mW cm⁻², bias = 5 V) and (f) gCN-*co*-gC 37% (420 nm, 120 mW cm⁻², bias = 5 V). EPR spectra of GCN (g) and gCN-*co*-gC 37% (h) without and with white light illumination. (i) Spin density of gCN and gCN-*co*-gC 37% dependent on illumination power.

enhanced electrical conductivity (Fig. 4c). For evaluating the electrical conductivity, we fabricated a device shown in Supplementary Fig. 6, where a gCN-co-gC film deposited on a glass substrate was covered with 18 sets of silver electrodes that were spaced 150 μ m apart from each other. Fig. 4c shows that, in the dark, the gCN-co-gC 37% film was five orders of magnitude more conductive than a reference gCN film.

gCN-co-gC could efficiently convert photons in the visible-light region to electrons, where gCN-co-gC 37% showed the best performance among all gCN-co-gC films fabricated in the present paper. Using monochromatic light (7 nm bandwidth) in the wavelength range of 300-600 nm, we investigated the wavelength dependency of gCN-co-gC on the photocurrent enhancement. Consistent with its electronic absorption profile (Figure 4a, orange), gCN-co-gC 37% showed the maximum photocurrent upon exposure to 420-nm visible light (Fig. 4d, orange), where the photocurrent increased from 0.28 nA to 105 reproducibly, (375-fold) even upon continuous photoexposure (Fig. 4f). In sharp contrast, although gCN showed a photocurrent enhancement upon exposure to 365 nm UV light (Fig. 4d, blue), the maximum photocurrent, as reported¹⁶, was considerably small (0.36 nA; Fig. 4e). gCN-cogC 50% in the dark was more conductive than gCN-co-gC 37% (Fig. 4c), but its photocurrent enhancement was only marginal (Fig. 4d, red), likely due to the structural disorder (Fig. 1d) caused by the excess amount of dopants^{17,18}.

We found that gCN-co-gC 37% upon exposure to a white light (AM 1.5 spectrum, 260 mW cm⁻²) displayed a Lorentzian shaped electron paramagnetic resonance (EPR) signal with a g value of 2.0044 (Fig. 4h, red). Note that the gCN-co-gC 37% showed the EPR signal even in the dark, in the air, and at room temperature. The radical is assignable to organic π radicals, which was previously reported in the range of 2.0027-2.0051 in gCN materials^{19,20}. We quantified the spin density of gCN-co-gC 37% using the integral of this EPR signal vs. that of a reference sample, CuSO₄•5H₂O. As shown in Fig. 4i (orange), the irradiation of gCN-co-gC 37% with the white light resulted in a nearly 4-times enhancement of the spin density from ~1.3 × 10^{15} spins mg⁻¹, observed in the dark, to ~5.3 × 10^{15} spins mg⁻¹. In sharp contrast, although gCN without gC domains (Fig. 4i, blue) showed a similar behaviour upon the white light exposure, its spin densities evaluated in the dark ($\sim 0.12 \times 10^{15}$ spins mg⁻¹) and under the light exposure ($\sim 0.70 \times 10^{15} \text{ spins mg}^{-1}$) were both much smaller than those of gCN-co-gC 37%. The radicals in gCN are not clearly observable in the dark but become observable under light irradiation, suggesting that they are photoexcited unpaired electrons and holes. In the meanwhile, radicals with the same resonance energy and linewidth are observed in gCN-co-gC even without light irradiation, strongly indicating that the gCN/gC boundary, i.e., open-shell non-Kelulé structure (Figs. 1b, 3c, 3f) has separated the electrons and holes, preventing their recombination.

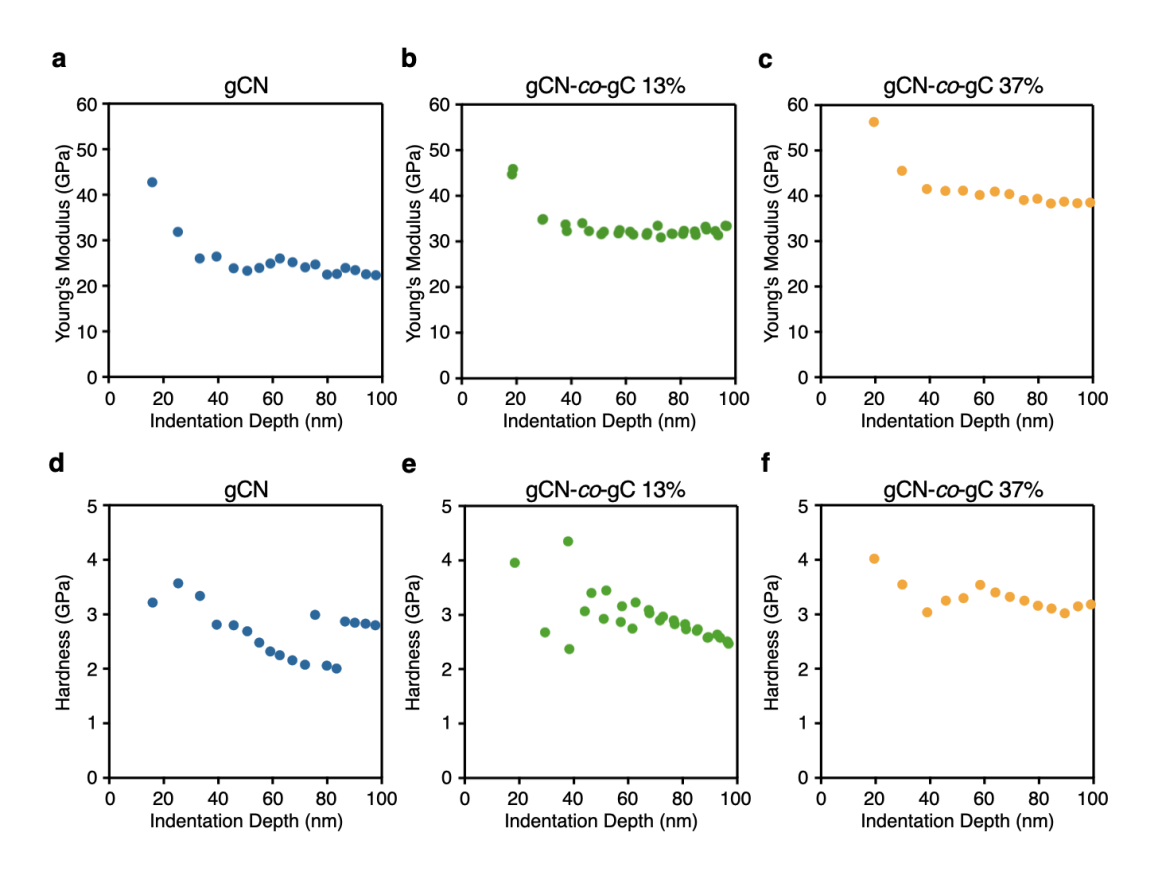


Fig. 5 | **Mechanical properties.** gCN, gCN-*co*-gC 13%, and gCN-*co*-gC 37% thin films are tested by nanoindentation. (a, b, c) Young modulus as a function of indentation depth. (d, e, f) hardness as a function of indentation depth.

Journal of Materials Chemistry C

An unexpected observation was that the mechanical toughness of the gCN-co-gC increased as the amount of gC increased (Fig. 5, Supplementary Fig. 12). gCN showed a Young's modulus of 24.6 GPa and a hardness of 2.3 GPa, as measured by nanoindentation testing. These values are closely aligned with those reported in a previous study⁶. On the other hand, gCN-co-gC 37% film exhibited higher mechanical strength, with a Young's modulus of 41.2 GPa and a hardness of 3.2 GPa. The measurement of crack onset strain showed that the incorporation of gC increased the crack onset strain, from 3% for gCN to 10% for the gCN-co-gC 37% (Supplementary Fig. 13). This film could be freestanding and also demonstrated its flexibility (Supplementary Video).

Conclusions

We have developed a straightforward method to produce gCN-co-gC films utilizing commonly available precursors in a dual-zone VDP setup. The precursors are composed of simple, low-risk, and economical chemicals. The morphology, optoelectronic, and mechanical properties can be easily tuned by adjusting the starting glucose concentration in the precursors. As the amount of gC increases in gCN-co-gC, mechanical toughness is enhanced. The gCN-co-gC exhibited narrow energy band gap and higher electrical conductivity than those of gCN films, and also retained stable radicals even without light irradiation. It could have various applications beyond photodetector, such as in photoelectrodes, spintronics, and solid-state lasers in the future.

Author contributions

N.M. and T.A. conceived the research. N.W. and N.M. designed and performed most of the experiments. S.M., Y.L.C. and X.Y. contributed to the HREM observation and STEM-EDS analyses. Y.O. contributed to the EPR measurements. S.W. and J.L. helped the photocurrent measurements. N.W., N.M., and T.A. wrote the manuscript with feedback from all authors.

Conflicts of interest

There are no conflicts to declare.

Data availability

The data supporting the findings of this study are available within the article and/or its ESI.

Acknowledgements

We thank Prof. Markus Antonietti (Max Planck Institute of Colloids and Interfaces) and Prof. Oleksandr Savateev (The Chinese University of Hong Kong) for salient point regarding the existence of radicals in gCN-co-gC, Mr. Motonobu Kuwayama (RIKEN) for discussion on chemical structure of gCN-co-gC, Dr. Kenichiro Itami (RIKEN) for the use of VDP apparatus, Dr.

Keisuke Tajima (RIKEN) and Dr. Kyohei Nakano (RIKEN) for the use of their XPS apparatus, Dr. Taishi Noma (RIKEN) for the use of photocurrent measurements setup, Dr. Hiroshi Sato (RIKEN) for the use of nanoindentation apparatus, Dr. Kiyohiro Adachi (RIKEN) for his help in XRD measurements, Dr. Kiyoshi Morishita (The University of Tokyo) for English proofreading, and also Kao Corporation for their generous support.

This work was financially supported by Grants-In-Aid for Scientific Research (Grant Nos. 21K04840 to N.M., 23H05408 to T.A., 22KJ0959 to N.W., 19H00660 to X.Y., 23K13639 and 22K20363 to S.M.) by the Japan Science and Technology Agency CREST program (Grant No. JPMJCR20T1 to X.Y.) and by RIKEN TRIP Initiative Polymer Chemistry.

References

- X. Wang, K. Maeda, A. Thomas, K. Takanabe, G. Xin, J. M. Carlsson, K. Domen and M. Antonietti, *Nat. Mater.* 2009, 8, 76–80.
- B. Zhu, L. Zhang, B. Cheng and Y. Jiaguo, Appl. Catal. B 2018, 224, 983–999.
- 3 E. Kabir, P. Kumar, S. Kumar, A. A. Adelodun and K. Kim, Renew. Sust. En. Rev. 2018, 82, 894–900.
- 4 C. Jia, L. Yang, Y. Zhang, X. Zhang, K. Xiao, J. Xu and J. Liu, ACS Appl. Mater. Interfaces, 2020, 12, 53571–53591.
- 5 H. Arazoe, D. Miyajima, K. Akaike, F. Araoka, E. Sato, T. Hikima, M. Kawamoto and T. Aida, Nat. Mater. 2016, 15, 1084–1089.
- 6 P. Giusto, D. Cruz, T. Heil, H. Arazoe, P. Lova, T. Aida, D. Comoretto, M. Patrini and M. Antonietti, Adv. Mater. 2020, 32. 1908140.
- 7 Y. Zhang, A. Thomas, M. Antonietti and X. Wang, *J. Am. Chem. Soc.* 2009, **131**, 50–51.
- 8 M. Volokh, G. Peng, J. Barrio and M. Shalom, *Angew. Chem. Int. Ed.* 2019, **58**, 6138–6151.
- 9 W. Che, W. Cheng, T. Yao, F. Tang, W. Liu, H. Su, Y. Huang, Q. Liu, J. Liu, F. Hu, Z. Pan, Z. Sun and S. Wei, J. Am. Chem. Soc. 2017, 139, 3021–3026.
- B. V. Lotsch, M. Döblinger, J. Sehnert, L. Seyfarth, J. Senker,
 O. Oeckler and W. Schnick, *Chem. Eur. J.* 2007, 13, 4969–4980.
- 11 Y. Yu, W. Yan, X. Wang, P. Li, W. Gao, H. Zou, S. Wu and K. Ding, Adv. Mater. 2018, 30, 1705060.
- 12 A. Thomas, A. Fischer, F. Goettmann, M. Antonietti, J.-O. Müller, R. Schlöglb and J. M. Carlsson, J. Mater. Chem. 2008, 18, 4893–4908.
- 13 Y. Baskin and L. Meyer, Phys. Rev. 1955, 100, 544.
- 14 H. Yu, R. Shi, Y. Zhao, T. Bian, Y. Zhao, C. Zhou, G. I. N. Waterhouse, L.-Z. Wu, C.-H. Tung and T. Zhang, Adv. Mater. 2017, 29, 1605148.
- 15 Y. Cui, D. Zhengxin, X. Fu and X. Wang, *Angew. Chem. Int. Ed.* 2012, **51**, 11814–11818.
- 16 Z. Liu, C. Wang, Z. Zhu, Q. Lou, C. Shen, Y. Chen, J. Sun, Y. Ye, J. Zang, L. Dong and C.-X. Shan, *Matter* 2021, 4, 1625–1638.
- 17 Y. Li, S. Zhu, Y. Liang, Z. Li, S. Wu, C. Chang, S. Luo and Z. Cui, Appl. Surf. Sci. 2021, 536, 147743.
- 18 W. Song, J. Wei, J. Lv, X. Cao, Y. Sun, S. Li, X. He, *Carbon* 2024, **228**, 119438.
- A. Actis, M. Melchionna, G. Filippini, P. Fornasiero, M. Prato, E. Salvadori and M. Chiesa, *Angew. Chem. Int. Ed.* 2022, 61, e202210640.
- 20 A. Actis, P. Fornasiero, M. Chiesa and E. Salvadori, ChemPhotoChem 2024, 8, e202300203.

Data availability

The authors confirm that the data supporting the findings of this study are available within the article and/or its ESI.